

# Transient temperature measurements of resist heating using nanothermocouples

Dachen Chu<sup>a)</sup>

*Integrated Circuits Laboratory, Stanford University, Stanford, California 94305*

Wai-Kin Wong

*Integrated Circuits Laboratory, Stanford University, Stanford, California 94305 and Department of Electrical and Computer Engineering, National University of Singapore, Singapore 119260, Singapore*

Kenneth E. Goodson

*Mechanical Engineering Department, Stanford University, Stanford, California 94305*

R. Fabian W. Pease

*Integrated Circuits Laboratory, Stanford University, Stanford, California 94305*

(Received 1 July 2003; accepted 15 September 2003; published 10 December 2003)

Resist heating is one of the major factors that causes feature size variation and pattern displacement in photomask fabrication. A number of models have been published to predict the rise in temperature during resist heating, but no transient temperature experimental results are available to verify those models. We have fabricated thin film gold/nickel thermocouples with junction areas as small as 100 nm<sup>2</sup> on silicon and 500 nm<sup>2</sup> on quartz. Microsecond scale transient resist heating measurements were obtained using these thermocouples. Irradiation by a 15 keV, 150 nA electron beam of 1.7 μm radius for 100 μs yielded temperature rises at the resist bottom surface of approximately 62 K on quartz substrates and of 18 K on silicon substrates. Simulation results using a multilayer Green's function model are in reasonable agreement with these experimental data for smaller temperature rises but tend to overestimate by about 10% for larger rises in temperature. In our experiments, a 100 ms exposure is equivalent to a dose of 150 μC/cm<sup>2</sup>. Under the same electron beam conditions electron dosages of 5 and 15 μC/cm<sup>2</sup> result in temperature rises of 25 and 40 K, respectively, on quartz substrates. © 2003 American Vacuum Society. [DOI: 10.1116/1.1624255]

## I. INTRODUCTION

The continuous shrinking of transistor critical dimensions (CDs) poses continual challenges to photomask makers to meet stringent CD tolerances. Resist heating was previously identified as one of the major contributors to errors in feature size and pattern placement.<sup>1-3</sup> During the past decade a number of authors have simulated resist temperature rise with different models and techniques.<sup>4-9</sup> However, experimental data to verify those models are scarce due to the difficulty in conducting transient temperature measurements with sufficient spatial and temporal resolution. Babin *et al.* measured the *in situ* temperature rise using a YBa<sub>2</sub>Cu<sub>3</sub>O<sub>7</sub> superconducting thermometer.<sup>10</sup> However, their experiments were conducted at liquid nitrogen temperatures, which do not replicate the real-life thermal environment in electron beam mask writing. Furthermore, the spatial resolution of the superconducting sensor used in the experiments was inadequate. Thin film thermocouple (TFTC) sensors are good candidates for such measurements due to their potential for small sensing volumes and junction areas, which allow higher spatial and temporal resolution and minimize distortion of the temperature field imposed by the sensor.

In previous work, we fabricated gold/nickel thermocouples with 400 nm<sup>2</sup> junction areas on silicon substrates using a lift-off process. The thermocouples were used to

measure steady-state temperature profiles during electron beam exposure.<sup>11</sup> In this article we report several improvements in resist heating measurements. First, the minimum junction area has been reduced to 100 nm<sup>2</sup> to achieve higher spatial resolution and less distortion in the temperature field during the measurements. Second, the TFTCs have been fabricated on quartz (fused silica) substrates (the same material used in photomasks) using a shadow mask process. Third, a beam blanker was added in our system to enable microsecond scale transient temperature measurements using the TFTCs under different conditions. The experimental results show reasonably good agreement with the multilayer Green's function model proposed earlier.<sup>6</sup>

## II. SAMPLE PREPARATION

Two fabrication techniques were developed to make the TFTCs. The first involves the lift-off process with the aid of electron beam lithography (EBL). Thermocouples with minimum junction areas of 200 nm×300 nm (Fig. 1) were fabricated on silicon substrates with 1 μm thick SiO<sub>2</sub> isolation layers. For some devices, a focused ion beam was used to surgically reduce the junction area to 100 nm×100 nm (Fig. 2). However, EBL is not suitable for patterning on nonconductive substrates due to electron beam charging issues. Hence a second technique that utilizes a shadow mask process was used to pattern fine metallic features on nonconductive substrates. The shadow mask process employs freestand-

<sup>a)</sup>Electronic mail: dcchu@stanford.edu

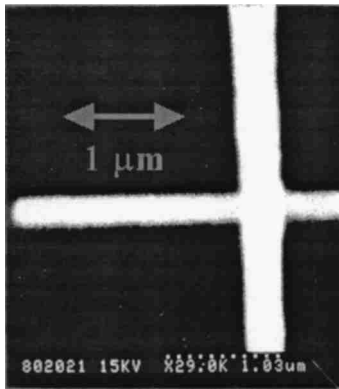


FIG. 1. Thermocouple junction 200 nm×300 nm patterned in gold and nickel using a lift-off process.

ing silicon nitride films (approximately 600 nm thick and up to 1 mm×1 mm membrane size) with slits patterned to the desired shapes. Slits with minimum 100 nm widths were drilled by focused ion beam milling to define the tip of the thermocouples. Two sets of shadow masks were made for the two layers of TFTCs. Alignment accuracy of about 2 μm was achieved using commercial aligners (EV group model 620). The fabrication steps are described in Fig. 3. Nickel and gold were evaporated through the shadow mask to form the pattern on quartz substrates.

The resultant width of the thermocouple tips prepared using the shadow mask process was found to broaden to 500 nm, compared to the 100–150 nm width of slits drilled on the shadow mask (Figs. 4 and 5). Two mechanisms contribute to feature size broadening. In the first mechanism, broadening is caused by warping of the silicon nitride membranes during the metal deposition step due to stress–strain buildup at the metal–nitride interface. The second mechanism is the penumbra effect due to the finite spacing (of the order of a few microns) between the quartz wafer and the shadow mask during the evaporation process. In both fabrication processes, a 3.5 nm chromium layer was deposited to promote adhesion prior to the deposition of nickel and gold. Since the chromium layers are much thinner than the gold (120 nm) and nickel (50 nm) layers, the effect of the chromium layers on the Seebeck coefficient of the thermocouple should not be significant. As an added precaution, we precalibrated these TFTCs before using them in the measurements. The calibra-

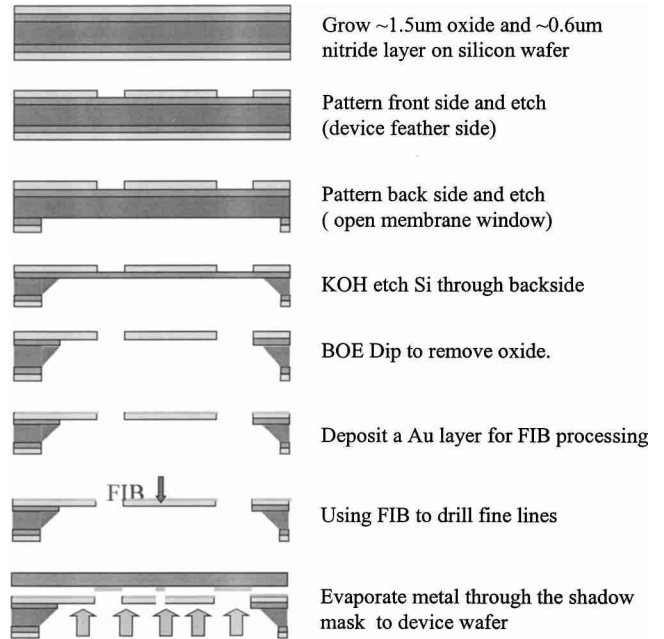


FIG. 3. Process flow of the patterning metallic feature using a shadow mask process.

tion procedures are described in Sec. III. After the TFTCs were fabricated, a 300 nm thick layer of PMMA was spin coated on top of the die for subsequent resist heating measurements.

### III. CHARACTERIZATION OF TFTCs

Conventionally thermocouples were calibrated by extending the junction off chip with wires made of the same materials. The reference junction was usually kept at a fixed temperature (for example, in ice water) off chip. The measurement junction was fabricated on chip and the temperature of the whole chip was controlled in an oven or on a hotplate during calibration. Thus this method essentially would calibrate the Seebeck coefficients of the extension wires (bulk value). To account for the differences in Seebeck coefficient between the thin film and bulk material, a special calibration structure was designed (Fig. 6). A gold line was patterned as a local joule-heating source. A resistive thermometer and the measurement junction of thermocouple were patterned at the exact same distance from the heater to

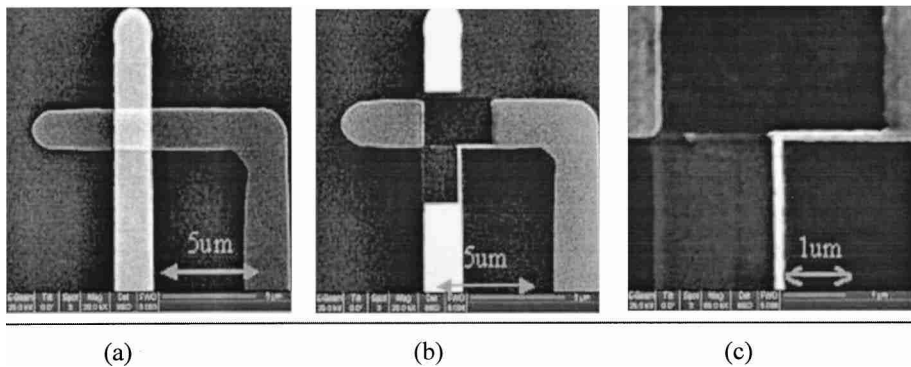


FIG. 2. Surgical reduction of a thermocouple junction using a FIB: (a) a 2 μm×2 μm junction; (b) a 100 nm×100 nm junction milled by FIB; and (c) the magnified junction part in (b).

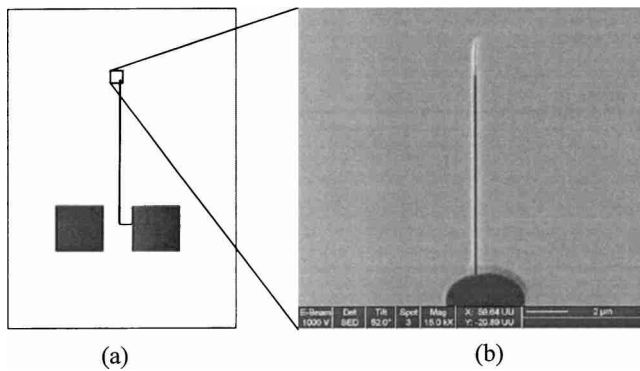


FIG. 4. Shadow mask made of a freestanding silicon nitride membrane. (a) Image of a shadow mask. (b) Magnified part of the tip, where the 150 nm slit was milled by a FIB.

ensure that both measure the same rise in temperature caused by the heater line. The reference junctions of the thermocouples were also on chip. But they were far away and thus not affected by the local heater line during calibration. In the temperature measurements, the resistive thermometer is first self-calibrated in a cryostat. Four-probe resistance measurements determine the temperature coefficient of resistance (TCR) of the gold resistor. The thermocouples are then calibrated against the resistive thermometer by applying current through the heater. In this article we used nickel and gold TFTCs with thicknesses of 50 and 120 nm, respectively. The measured Seebeck coefficients range from 6 to 7  $\mu\text{V}/\text{K}$ . The uncertainty in the calibration was estimated to be less than 10%.

The transient response of the thermocouples was characterized by laser flash heating.<sup>12</sup> A 10 ns Nd:YAG laser pulse was used to heat the TFTC junction and the corresponding TC signal was amplified and recorded to characterize the temporal resolution of the TFTC. The temporal response time of the TFTC is defined as the time it takes for the thermocouple output to rise from 10% to 90% of its peak value. Response times of less than 400 ns were obtained using the experimental arrangement shown in Fig. 7.

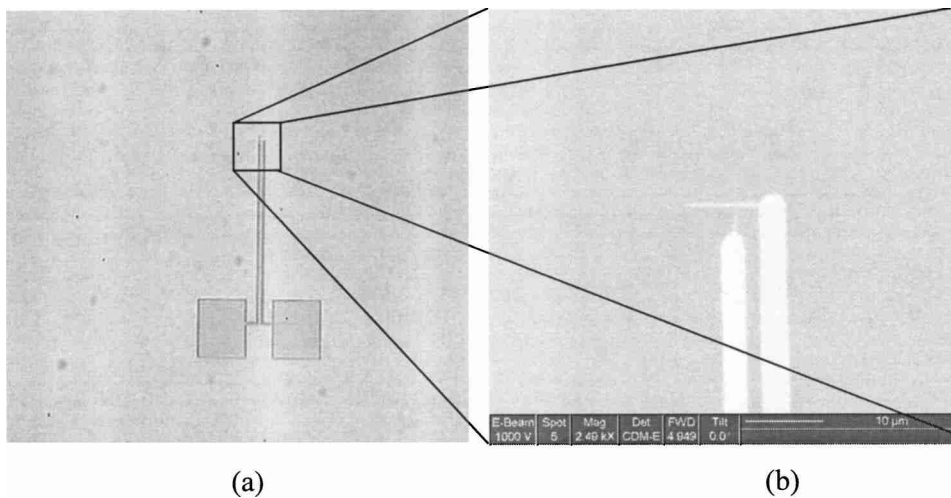


FIG. 5. Gold/nickel thermocouple patterned on a glass substrate using the shadow mask process. (a) Image of the thermocouple. (b) Magnified part of the junction.

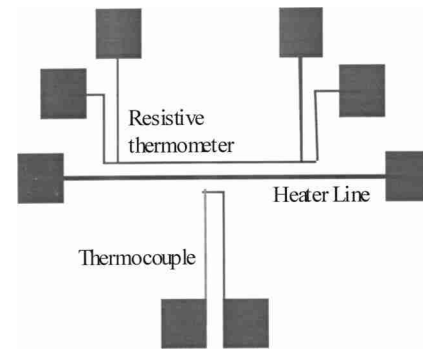


FIG. 6. Layout of the structure for thermocouple calibration (not to scale).

## IV. TRANSIENT TEMPERATURE MEASUREMENTS OF PMMA RESISTS

### A. Experimental procedure

*In situ* temperature measurements were carried out on a Hitachi S2500 scanning electron microscope equipped with a tungsten thermionic gun and a beam blanker capable of delivering primary electron beam pulses with rise and fall times under 100 ns. A low duty cycle (10%) TTL reference signal was applied to the beam blanker to pulse the electron beam. The corresponding thermocouple output was amplified by a voltage amplifier (SRS™ SR570) and then recorded on a digital storage oscilloscope (Tektronix™ TDS 460A) (Fig. 8). TFTCs were used to measure temperature rise in the resist of both the silicon and quartz substrates. The silicon substrate of the test dies was electrically grounded during the measurements to mitigate electron beam charging effects. Because quartz substrates are poor electrical conductors, a 60 nm thick aluminum followed by a 1000 nm thick low temperature oxide (LTO) isolation layer were predeposited on the quartz substrate prior to the fabrication of TFTCs. During the *in situ* measurements the aluminum layers were grounded.

Experiments were conducted to ensure that only thermal effects contribute to the thermocouple signal, and that there

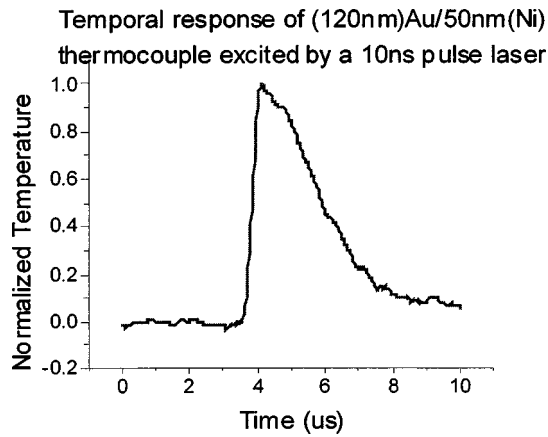


FIG. 7. Transient temperature response of a Au (120 nm)/Ni (50 nm) thermocouple under 10 ns laser heating. The rise time is less than 400 ns.

is negligible electrical coupling from the power source of the primary electron beam. This was accomplished by using a “dummy” thermocouple junction fabricated on the same chip that consisted of a single material which was designed to yield a zero thermal signal. When the beam was scanned across the dummy junctions, no appreciable output from the dummy thermocouple was detected, thereby supporting the conclusion that purely electrical signals are negligible. Similarly, no signal was observed when the beam was scanned across the arms of the TFTC away from the thermocouple junction regions. However, the primary electron beam does increase the noise level significantly in the transient heating measurements compared to in laser heating measurements. This intrinsic source of noise limits the temporal resolution of our temperature measurements.

Experiments were carried out using different thermocouples on both quartz and silicon substrates. The electron beam was assumed to take on a Gaussian shape,

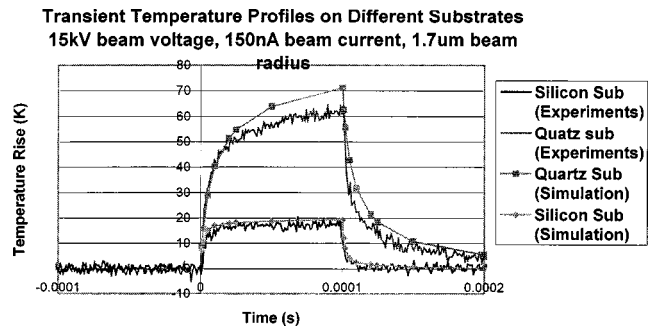


FIG. 9. Experimental and calculated temperature profiles of the bottom surface of resist on both silicon and quartz substrates (a 1 μm oxide layer exists between the TFTCs and the substrates), irradiated by a 15 keV Gaussian beam. The beam current is 150 nA and the beam radius is 1.7 μm.

$$j(r) = \frac{i_b}{2\pi r_b^2} \exp\left(\frac{-r^2}{2r_b^2}\right),$$

where  $i_b$  represents the beam current and  $r_b$  represents the beam radius where current density  $j$  falls to 60.9% of its maximum value. In experiments we measured  $i_b$  and  $r_b$ , respectively, using a picoammeter and a knife-edge structure.

### B. Results and discussion

The results are summarized in Fig. 9. Here, temperature rises at the PMMA/oxide interface on a silicon substrate were compared with those on a quartz substrate. Under the experimental conditions of a 15 keV primary electron beam with 1.7 μm beam radius and total current of 150 nA, we observe a peak temperature rise of approximately 18 K on a silicon substrate and of 62 K for the case of a quartz substrate within a 100 μs exposure window. In the silicon substrate case, the temperature rise achieved a steady-state value within 10 μs, whereas in the case of quartz the temperature was observed to rise continuously with electron beam irra-

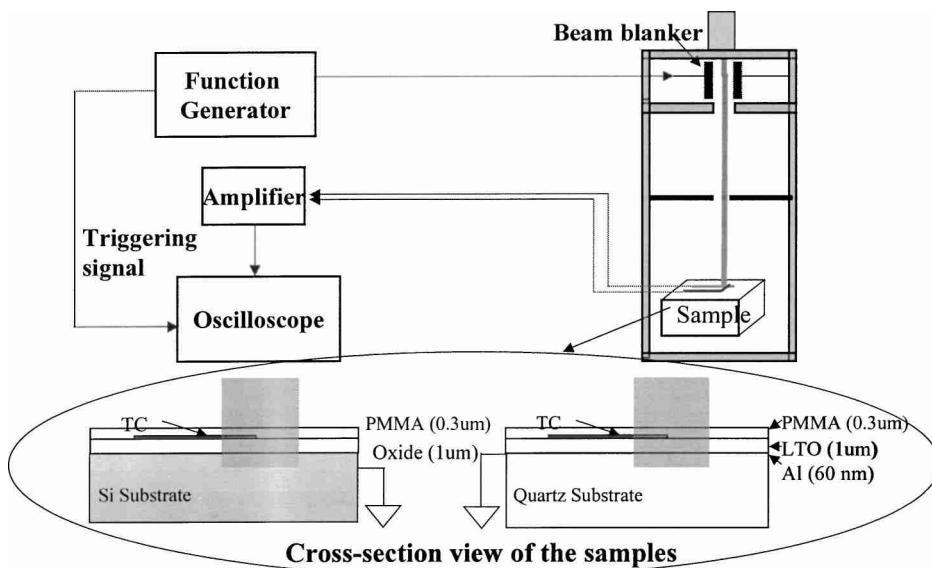


FIG. 8. Experimental diagram. A TTL reference signal was used to turn the electron beam on and off. The resultant TFTC signals were recorded after amplification. TFTCs on both silicon and quartz substrates were used in the measurements. Cross-sectional views that show details of the structure of the samples.

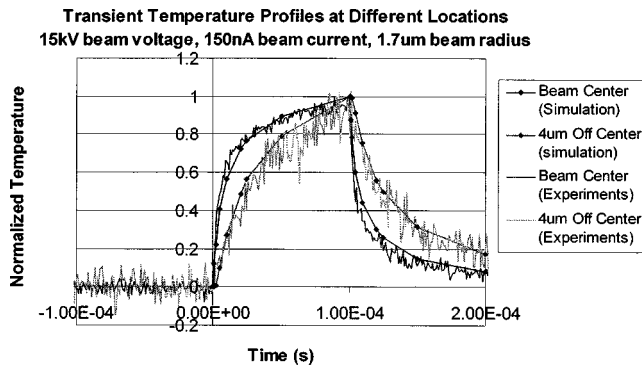


FIG. 10. Normalized experimental and simulation temperature profiles of the bottom surface of resist on the quartz substrate at two different locations from the center of the electron beam. The beam conditions are the same as in Fig. 9.

diation. This is due to the significant difference in thermal conductivity value between silicon (148 W/m K) and quartz (1.4 W/m K).

In our experiments the average beam current density is  $1.5 \text{ A/cm}^2$ . Therefore a  $100 \mu\text{s}$  exposure time corresponds to a  $150 \mu\text{C/cm}^2$  electron dose. From interpolation of the quartz substrate temperature curves in Fig. 9, doses of 5 and  $15 \mu\text{C/cm}^2$  would result in temperature rises of 25 and 40 K, respectively. The temperature increases sharply at the onset of electron exposure, since the initial heat transfer mechanism is adiabatic. Subsequently, the temperature settles to a steady-state value once a stable temperature gradient is established in the structure and the rate of heating equals the rate of heat sinking. As expected, the decay time constant on a quartz substrate was measured to be more than an order of magnitude longer than that on a silicon substrate.

The experimental data for the silicon substrate are in good agreement with results using the multilayer Green's function model proposed earlier. However, for the quartz substrate, the modeling results tend to overestimate the temperature rise. One possible reason is the contribution of nonlinear effects such as changes in thermal conductivity with the temperature which was not accounted for in the Green's function model. More likely explanations are the uncertainty in the beam radius measurements (about 10%) and discrepancies between the energy profile used in the model and that in actual experiments.

Temperatures were also measured on the quartz both at the electron beam axis and  $4 \mu\text{m}$  off axis (Fig. 10). The

normalized curves were plotted against the modeling results and the experimental results are shown to closely fit the theoretical data. Furthermore, the good agreement in the rise and fall time constants of the dynamic heating further increases our confidence in the validity of the Green's function model as applied to modeling of resist heating.

## V. SUMMARY AND CONCLUSIONS

Gold/nickel thin film thermocouples with 100 nm minimum junction size were fabricated on silicon and quartz substrates. Microsecond scale *in situ* temperature measurements were performed which indicate that resist heating is more than three times higher for quartz substrates compared to silicon substrates with  $1 \mu\text{m}$  thick oxide isolation layers in both cases. The heat transfer mechanism is adiabatic at the beginning of exposure (corresponding to a linear increase in temperature) and gradually saturates to steady state, during which heat conduction through the substrate is dominant. The results are consistent with a solution to the transient heat conduction equation based on the Green's functions which we developed and reported earlier.<sup>6</sup>

## ACKNOWLEDGMENTS

This work was supported financially by Intel and SRC via Contract No. MJ-653. The authors are grateful to Dr. Qian Wang for his help in shadow mask processes and Fu-Chang Lo and the Stanford Mask Advisory Group for their valuable guidance.

- <sup>1</sup>E. Kratschmer and T. Groves, *J. Vac. Sci. Technol. B* **8**, 1898 (1990).
- <sup>2</sup>M. Yasuda, H. Kawata, K. Murata, K. Hashimoto, Y. Hirai, and N. Nomura, *J. Vac. Sci. Technol. B* **12**, 1362 (1994).
- <sup>3</sup>S. Babin, *J. Vac. Sci. Technol. B* **15**, 2209 (1997).
- <sup>4</sup>H. Ralph *et al.*, *Proceeding of the 10th International Conference on Electron and Ion Beam Science and Technology*, 1982, p. 219.
- <sup>5</sup>T. R. Groves, *J. Vac. Sci. Technol. B* **14**, 3839 (1996).
- <sup>6</sup>D. Chu, R. F. W. Pease, and K. Goodson, *Proc. SPIE* **4689**, 206 (2002).
- <sup>7</sup>T. Abe, K. Ohta, H. Wada, and T. Takigawa, *J. Vac. Sci. Technol. B* **6**, 853 (1988).
- <sup>8</sup>E. V. Drift, A. C. Enters, and S. Radelaar, *J. Vac. Sci. Technol. B* **9**, 3470 (1991).
- <sup>9</sup>S. Babin, I. Y. Kuzmin, and G. Sergeev, *Proc. SPIE* **2884**, 520 (1996).
- <sup>10</sup>S. Babin, M. E. Gaevski, and S. G. Konnikov, *J. Vac. Sci. Technol. B* **19**, 153 (2001).
- <sup>11</sup>D. Chu, D. T. Bilir, K. E. Goodson, and R. F. W. Pease, *J. Vac. Sci. Technol. B* **20**, 3044 (2002).
- <sup>12</sup>D. Burgess, Jr., M. Yust, and K. G. Kreider, *Sens. Actuators A* **29**, 155 (1990).